JOURNAL OF GEOPHYSICAL RESEARCH, VOL. 101, NO. D2, PAGES 4033–4040, FEBRUARY 20, 1996

Atomic hydrogen and ozone concentrations derived from simultaneous lidar and rocket airglow measurements in the equatorial region

Hisao Takahashi, Stella. M. L. Melo, B. R. Clemesha, and D. M. Simonich

Instituto Nacional de Pesquisas Espaciais, INPE, São José dos Campos, Brazil

J. Stegman and G. Witt

Department of Meteorology, Stockholm University, Sweden

Abstract. Nighttime atomic hydrogen and ozone concentrations are derived from simultaneous measurements of the vertical profiles of upper mesospheric airglow emissions and atmospheric sodium. The airglow profiles were obtained in a sounding rocket experiment launched from Alcântara (2.5°S, 44.2°W) on May 31, 1992. A lidar operating at the launch site was used to measure sodium at the time of the rocket experiment. A total of 10 airglow photometers, 6 forward looking and 4 side looking, observed the OI 557.7 nm, O_2 Herzberg and O_2 atmospheric (0,0) bands, sodium D lines, OI 630 nm, OH(8,3) band, and the airglow continuum. The simultaneous ground-based sodium lidar and onboard sodium airglow measurements made it possible to derive the ozone concentration at heights between 85 and 100 km. The hydrogen concentrations were then calculated from the O_2 atmospheric (0,0), OH(8,3), and the ozone profiles. The results suggest that the hydrogen concentration varied from 1×10^9 cm^{-3} at 85 km to 1×10^8 cm^{-3} at 100 km, values much higher than those suggested by recent model atmospheres and by some rocket observations at middle and high latitudes. Although the method of obtaining the concentrations of the minor constituents in the upper atmosphere is an indirect optical technique, this is the first time that these concentrations have been measured by rocket in the equatorial region.

1. Introduction

Atomic oxygen, ozone, and atomic hydrogen are the main species that control photochemical processes in the upper mesosphere and the lower thermosphere between 80 and 120 km. To understand the behavior of these species, in terms of day-to-day and seasonal variations, dependence on latitude and height, it is very important to investigate not only the photochemical processes involved but also the dynamical processes that occur in this altitude range. The height profiles are highly dependent on vertical mixing processes and meridional circulation [*Garcia and Solomon*, 1985]. Observation and monitoring of these species, however, is still very limited, owing to the technical difficulties involved.

Atomic oxygen has been measured by the resonance lamp technique on board a rocket [*Dickinson et al.*, 1980]. Several rocket measurements have been carried out using this technique together with oxygen airglow measurements [*Thomas and Young*, 1981; *Greer et al.*, 1986]. Through these experiments, it has been possible to obtain empirical values for the transition probabilities and quenching coefficients required to derive atomic oxygen concentration from airglow emissions [*Murtagh et al.*, 1990]. Today, the oxygen-related airglow emissions are used to calculate the concentration of atomic oxygen, using the OI 557.7 nm and O_2 atmospheric band emissions for the height range 85 to 110 km and hydroxyl band emissions for below 90 km [*McDade and Llewellyn*, 1988].

Daytime ozone concentration can be obtained from measurements of the $O_2(^1\Delta)$ 1.27 μm emission which results from ozone photolysis by solar ultraviolet radiation. During the nighttime, on the other hand, the only direct measurement technique available is to measure the infrared radiation from ozone [*Grossman et al.*, 1987]. The results of indirect measurements, using lidar profiles of sodium density together with airglow measurements of the 589 nm emission, have been presented by *Kirchhoff et al.* [1981], *Takahashi, et al.*, [1992], and *Clemesha et al.* [1993].

Atomic hydrogen is one of the more difficult species to measure directly in the upper atmosphere. Hitherto, using a direct technique, only one rocket measurement has been carried out by *Sharp and Kita* [1987]. Using an indirect technique, *Thomas* [1990a] derived hydrogen concentrations from the ozone density and the OH airglow intensity determined from the SME satellite data. *Takahashi et al.* [1992] used a similar technique to estimate hydrogen using ground-based observations. *Adler-Golden et al.*[1992] measured infrared ozone ν_3 band emissions by rocket and succeeded in deriving O and H atom concentration profiles.

In the present study, ozone concentration is first inferred from profiles of the NaD emission and the Na density, measured by rocket-borne photometers and lidar, respectively.

Paper number 95JD03035.
0148-0227/96/95JD-03035$05.00

Subsequently, hydrogen concentration is calculated in two ways: one from the ozone concentration and the atomic oxygen concentration inferred from the O_2 atmospheric (0,0) band and the other from the ozone concentration and the OH (8,3) emission profile. This is the first combined ground-based and rocket experiment from which it has been possible to estimate nighttime ozone and hydrogen concentrations in the equatorial mesopause region.

2. Experiments

The MULTIFOT payload, which included six forward looking and four side looking airglow photometers and two ionospheric plasma probes, was launched by a SONDA III rocket from the Alcântara Launch Center (2.5°S, 44.2°W), at 2352 Local Standard Time on May 31, 1992. During its 12 min flight the payload reached an altitude of 282 km and traveled a horizontal distance of 398 km.

The purpose of the experiment was to measure the vertical profiles of the O_2 Herzberg, O_2 atmospheric (0,0), and OH(8,3) bands together with the OI 557.7 nm and NaD 589.3 nm emissions between 80 to 120 km in the upper mesosphere and lower thermosphere. A 578 nm forward looking photometer was used to estimate the background airglow continuum. The data used in the present study were from the forward looking NaD 589.3 nm, OH(8,3) 724 nm R branch, and BG 578 nm photometers. The photometer specifications are shown in Table 1.

The photometer spectral and absolute sensitivities were calibrated in the laboratory using a laboratory standard (Eppley 100W) lamp and MgO white diffuser. The photometers included tritium-activated light sources to check their sensitivities during the flight. No changes from the preflight values were detected.

Measurements of the atomic sodium concentration were made using a lidar system installed approximately 5 km from the launch ramp. Information on the lidar measurements and conditions of observation during the flight can be found in the work of *Clemesha et al.* [1993].

3. NaD and OH(8,3) Emission Profiles

During the upleg passage through the emission region the OH(8,3) and O_2 atmospheric (0,0) band photometers suffered strong extraneous noise contamination, which started before the nose cone opened and lasted for about 50 s, after which time it disappeared completely. This made it impossible to reduce the upleg data from these two photometers. However, neither the NaD 589.3 nm photometer nor the BG 578 nm photometer suffered any noise contamination. During the downleg passage, contamination was detected from none of the photometers. This was concluded from the fact that the wideband (10 nm) BG 578 nm photometer showed similar signals during upleg and downleg passages through the emission region and did not show any unexpected variations in intensity. In the present experiment, no obvious light contamination, such as the vehicle glow observed by *Clemesha et al.* [1987], was detected. Although the same type of rocket (SONDA III) was used, the payload configuration was totally different, and the vehicle velocity was much lower. Because of the extraneous upleg signals observed from the infrared photometers, only the downleg data will be used in calculating the volume emission rates used in the present study.

Table 1. Rocket-Borne Photometer Specifications

Photometer	λ, nm	Δλ, nm	PMT	Sensitivity *
O_2 Herzberg	275.0	14.3	EMI 9924	191.0
OI 5577	557.7	1.7	EMI 9924	684.0
BG 578	578.0	11.0	EMI 9924	220.2
NaD 5893	589.0	1.7	EMI 9924	326.9
OH(8,3)	724.2	1.9	EMI 9798	143.9
O_2 atm. (0,0)	762.0	5.7	EMI 9798	43.6

Photometer field of view: 4° (half angle); optical diameter of objective lens: 46 mm; orientation: forward looking (parallel to the rocket axis).

*Counts s^{-1} $Rayleigh^{-1}$.

To determine the intensity of the NaD (D_1+ D_2) emission, it is necessary to take into account spectral contamination from the OH(8,2) Q branch and the airglow continuum superposed in the filter passband. The contribution of OH(8,2) was calculated using the observed OH(8,3) band intensity with an appropriate instrumental factor and the ratio of the relevant transition probabilities. The continuum contribution in the 589 nm region was estimated by using an appropriate fraction of the continuum intensity observed at 578 nm. The OH(8,2) contribution to the 589.3 nm photometer signal was found to be 21% at the peak of the OH emission layer, and the continuum emission contributed a maximum of 11% at a height of 85 km. The NaD volume emission profile obtained in this way for the downleg is plotted in Figure 1. An incremental straight line fitting technique [*Murtagh et al.*, 1984] with a 4 km fitting length was used to smooth the profile.

Figure 1 also shows the lidar sodium profile. It can be seen that the profiles of airglow volume emission rate (proportional to the concentration of excited sodium) and the Na density (proportional to the density of ground state sodium) are fairly similar, with sharp boundaries both at the bottom and at the top of the layers. In this context it should be remembered that the two profiles refer to regions separated by a horizontal distance of approximately 300 km.

In the case of the OH(8,3) R branch, spectral contamination at 724 nm from the airglow continuum was estimated from the continuum observed at the 578 nm region. To estimate the ratio between the intensities in the 724 nm and 578 nm regions, we used data from the ETON campaign [*McDade et al.*, 1986b], leading to the adoption of a value of 1.33 for $I_{(724)}/I_{(578)}$. This ratio, however, could be height dependent. According to *McDade et al.*[1986b] it could vary from 1.0 to 2.0 between 90 and 100 km. However, the error due to this uncertainty should be negligible in the present study. The contribution of the continuum to the OH(8,3) photometer signal was around 8% of the total output. The uncertainty originating from the continuum subtraction, therefore, should be less than 3%, which is less than the experimental error from other sources. The resulting OH(8,3) emission profile is shown in Figure 2. The peak height is around 87 km with a half-width of approximately 10 km. The observed integrated intensity, 550 Rayleigh, is somewhat higher than expected. A ground-based photometer at the launch site measured an OH(9,4) band intensity of about 700 R. On the basis of the intensity ratio of 1.6 for $I_{(9,4)}/I_{(8,3)}$, obtained by *Takahashi and Batista* [1981], the OH(8,3) intensity should be around 440 R. However recent ground-based observation carried out by *Johnston and Broadfoot* [1993] showed similar intensity levels for the OH(9,4) and OH(8,3) bands. If this is correct, our present results, suggesting an intensity ratio of 1.3, are not surprising.

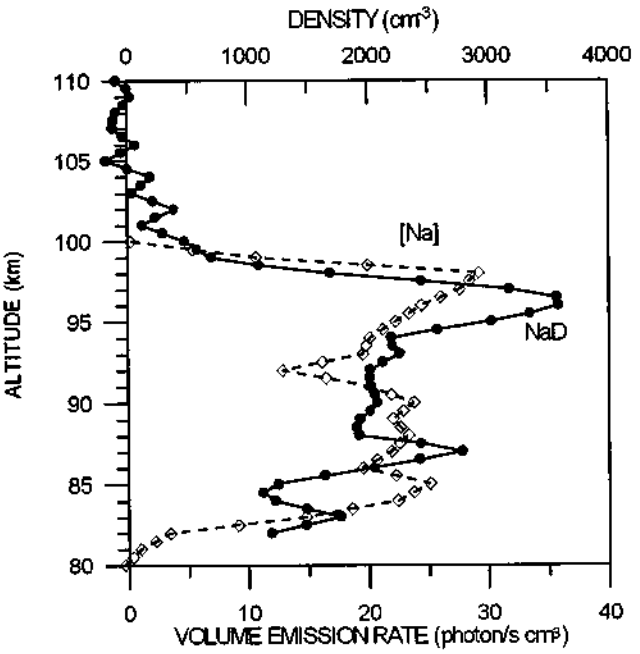

Figure 1 NaD volume emission rate measured by rocket and the Na atom concentrations measured by ground-based lidar, both for the Alcântara launch site, May 31, 1992.

It could be that latitudinal or local differences in photochemical equilibrium lead to differences in the OH vibrational distribution.

One of the side looking photometers in the present payload also measured the OH(8,3) band intensity. Since the payload rotation caused the side looking photometers to scan the emission layers, these instruments provided information on horizontal variations in emission intensity. An analysis of the data from the side looking photometers [*Clemesha and Takahashi*, 1995] has shown variations by nearly a factor of 2 occurring over a horizontal distance of little more than 100 km, in the region of the downleg passage of the payload through the emitting region. For this reason it cannot be ruled out that the relatively high OH(8,3) integrated intensity was due to local variations in the emission intensities. It should be pointed out, however, that the OI 557.7 photometer showed significant differences in neither the integrated intensities nor the emission rate profiles between upleg and downleg.

4. Ozone Concentration

It is generally accepted that the sodium nightglow emission results mainly from the Chapman mechanism [*Chapman*, 1939],

$$Na + O_3 \rightarrow NaO + O_2 \quad k_1 \qquad (1)$$

$$NaO + O \rightarrow Na(^2P) + O_2 \quad \alpha\, k_2 \qquad (2)$$

It is conceivable that other mechanisms exist for the production of Na(^{2}P). However, there is no reason to believe that any of these make a significant contribution to the NaD airglow emission. The NaD volume emission rate is directly related to the rate of production of Na(^{2}P) via equation (2), and since the processes of oxidation (1) and reduction (2) are very rapid and in quasi-equilibrium, the NaD emission rate is equal to

$$V_{(NaD)} = k_1\, \alpha\, [Na][O_3] \qquad (3)$$

where k_1 and k_2 are chemical reaction rates and the branching ratio, α, is the fraction of Na atoms produced in the (^{2}P) state. The brackets indicate number densities. The radiative lifetime of Na(^{2}P) is so short (nanoseconds) that there can be no significant quenching. Therefore given the atomic sodium and NaD emission profiles, and values for k_1 and α, the ozone concentration (hereinafter $[O_3]$) can be determined.

There is some consensus of opinion concerning the absolute value of k_1 [*Worsnop*, 1991, *Plane et al.*, 1993]. However, this is not true in case of the branching ratio α. Laboratory measurements by *Plane and Husain* [1986] have indicated values less than 0.01, and *Bates and Ohja* [1980] suggested a value of around 0.3. Recent theoretical work by *Herschbach et al.*[1992] suggests a much higher value, around 0.67. This value is based on the possibility that NaO is produced in an electronically excited state and that the excess energy leads to a higher yield for excited Na than is observed in laboratory measurements. On the other hand, there is no experimental evidence for this hypothesis. It is more plausible that the excess chemical energy in reaction (2) would go to a newly formed O_2 bond. Recent work by *Plane et al.*[1993] and *Clemesha et al.*[1995] suggests that the fraction should be much smaller than that suggested by Herschbach and that it should be around 0.1. In view of this uncertainty, we have calculated ozone concentrations for what appear to be reasonable limiting values of 0.1 and 0.67. The adopted reaction rates and other parameters are listed in Table 2. The ozone profiles calculated in this manner are shown in Figure 3.

As expected from the similarity between the height profiles of NaD and Na shown in Figure 1, the calculated O_3 profiles in Figure 3 do not show the clear peak seen in model atmospheres [e.g., *Allen et al.*,1984]. In the case of α=0.1, the concentration varies from 1×10^8 cm^{-3} at around 85 km to 2.5×10^8 cm^{-3} at around 95 km.

In the paper by *Clemesha et al.* [1993] the O_3 profile was inferred from the same rocket experiment but using the upleg NaD profile and a value of 0.67 for α. In the absence of upleg

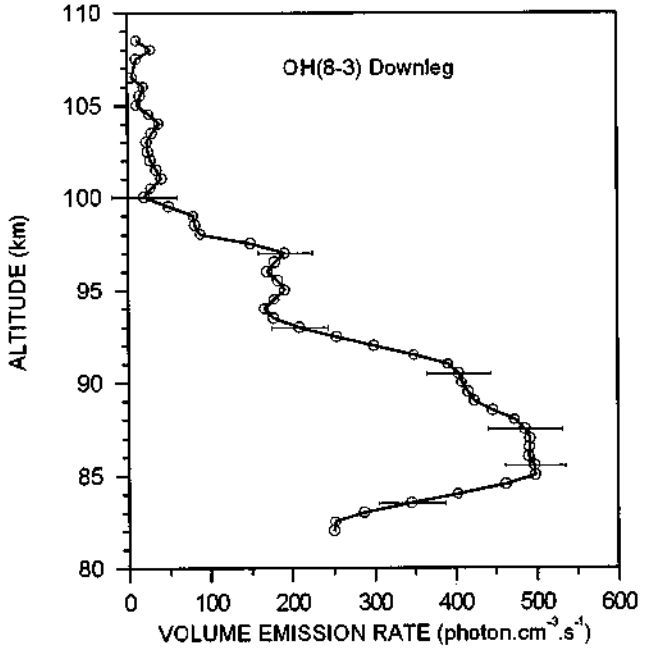

Figure 2 OH (8,3) band volume emission rate observed from Alcântara, May 31, 1992.

Table 2. Reactions and Adopted Parameters

Reaction	Rate	Reference
(1) $Na + O_3 \rightarrow NaO + O_2$	$k_1 = 1.6 \times 10^{-9} \exp(-195/T)$	Worsnop et al.[1991]
(2) $NaO + O \rightarrow Na(^2P) + O_2$	$\alpha \leq 0.1$	Kolb and Elgin[1976]
	$\alpha = 0.3$	Bates and Ojha[1980]
	$\alpha = 0.67$	Herschbach et al.[1992]
(4) $O + O_2 + M \rightarrow O_3 + M$	$k_{4(N2)} = 5.7\times10^{-34}(T/300)^{-2.62}$	Lin and Leu [1982]
	$k_{4(N2)} = 5.7\times10^{-34}(T/300)^{-2.62}$	Lin and Leu [1982]
(5) $O_3 + H \rightarrow OH^*(v) + O_2$	$k_5 = 1.4\times10^{-10} \exp(-470/T)$	DeMore et al. [1987]
(6) $O_3 + O \rightarrow O_2 + O_2$	$k_6 = 8.0\times10^{-12} \exp(-2060/T)$	DeMore et al. [1987]
A(8)/A(8,3) = 320		Murphy[1971]
A(8)/A(8,3) = 118		Turnbull and Lowe [1989]
f(9) = 0.32		Ohyama et al. [1985]
f(8) = 0.29		Ohyama et al. [1985]
$A(9)/k_{O2}(9) = 5.8 \times10^{12}$		see text

data from the forward looking 724.2 nm photometer, the contribution of OH(8,2) to the 589.3 nm photometer signal was estimated from the OH(8,3) intensity measured by one of the side looking photometers. In the presence of strong horizontal gradients this could result in an error in estimating the contribution of the OH(8,2) emission. In the present work we will use the OH(8,3) band intensity, together with the ozone profile, to estimate the hydrogen concentration. For this reason it was preferred to use the downleg NaD and OH profiles, both derived from forward looking photometers. Although this means that the ozone is derived from Na and NaD profiles measured at locations separated by about 300 km, as discussed later, we do not believe that this introduces an important error. It should be noted that the ozone distribution derived in the present analysis, profile b in Figure 3, does not differ greatly from that presented in the earlier paper.

5. Hydrogen Concentration

Although the photochemistry of oxygen and hydrogen in the upper mesosphere and lower thermosphere is complex, the equilibrium between atomic hydrogen and ozone can be expressed simply. The main ozone production process is

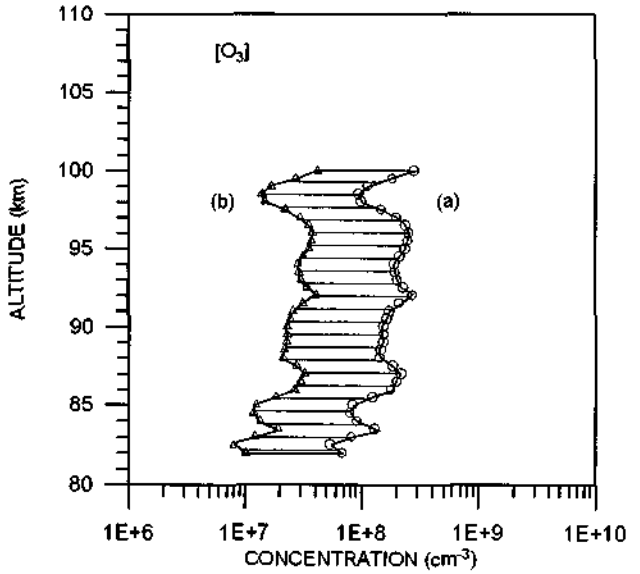

Figure 3 Inferred ozone concentrations for (a) $\alpha = 0.1$; (b) $\alpha = 0.67$.

$$O + O_2 + M \rightarrow O_3 + M \quad k_4 \qquad (4)$$

There are two ozone loss processes:

$$O_3 + H \rightarrow OH^*(v) + O_2 \quad k_5 \qquad (5)$$

which is the main loss process, producing vibrationally excited OH, and

$$O_3 + O \rightarrow O_2 + O_2 \quad k_6 \qquad (6)$$

which is slow compared to reaction (5) but becomes non negligible above 95 km.

From the photochemical equilibrium of ozone in equations (4), (5), and (6) the hydrogen concentration (here in after **[H]**) can be calculated as

$$[H] = \frac{k_4[O][O_2][M]}{k_5[O_3]} - \frac{k_6}{k_5}[O] \qquad (7)$$

Therefore if [O], $[O_2]$, $[O_3]$, and [M] are given, [H] can be calculated.

In the present work, [O] was derived from the O_2 atmospheric (0,0) band volume emission rate profile observed by the same payload. The details of how this was done are presented by *Melo et al.*[1995]. The resulting atomic oxygen profile is shown in Figure 4. Also shown in Figure 4, for comparison, is an [O] profile computed from the MSIS model for the appropriate input conditions. It is noted that the present [O] profile is in some agreement with the model, not showing any anomalous feature. Temperature and the O_2 and N_2 profiles were taken from the CIRA-86 model for heights up to 90 km and the MSIS model for greater heights. The CIRA and MSIS temperatures were adjusted to agree with the OH rotational temperature measured by the ground-based photometer at the time of the launch, and the major constituent profiles were adjusted to maintain hydrostatic equilibrium. The results for the hydrogen concentrations are shown in Figure 5. Curve a in this figure corresponds to the case of ozone formation with the fraction $\alpha = 0.1$. Curve c corresponds to $\alpha = 0.67$.

The hydrogen concentration can also be calculated by using $[O_3]$ and the observed OH(8,3) band intensity. Following *McDade et al.* [1987], the OH(8,3) band volume emission rate, V_{83}, is given by

$$V_{83} = \frac{A_{(8,3)}k_5[H][O_3]}{L(8)}\left[f(8) + f(9)\frac{A_{(9,8)} + \sum_Q k_Q(9,8)[Q]}{L(9)}\right] \qquad (8)$$

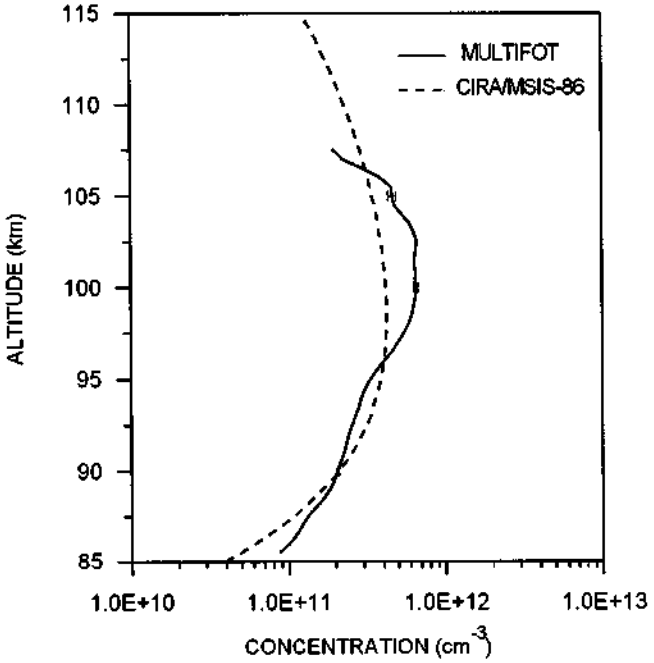

Figure 4 Atomic oxygen concentrations obtained from the observed O_2 atmospheric (0,0) band volume emission rate, compared with an [O] profile from the MSIS model.

where f(8) and f(9) represent the fractions of OH excited into the vibrational levels 8 and 9, respectively, and L(8) and L(9) represent the total losses from these levels; that is,

$$L(v)=A(v)+\Sigma_Q k_Q(v)[Q] \qquad (9)$$

where A(v) is the vibrational transition probability of level v, and Q is the quenching agent, mainly N_2 and O_2.

For the vibrationally excited OH quenching process, *McDade et al.* [1987] considered two different schemes, sudden death and collisional cascade. The former assumes that any collisional deactivation of the vibrationally excited OH causes its total energy loss immediately, i.e., from v to v = 0. On the other hand, the latter assumes that the collisional deactivation causes only one step vibrational cascading, i.e., from v to v-1. Therefore in the case of the sudden death model, the term "$k_Q(9,8)$" in equation (8) is equal to zero,

$$V_{83}=\frac{A_{(8,3)}k_5[H][O_3]}{L(8)}\left[f(8)+f(9)\frac{A_{(9,8)}}{L(9)}\right] \qquad (10)$$

As pointed out by *McDade et al.* [1987], the term f(9)A(9,8)/L(9) is considerably smaller than f(8), so it can be neglected. Therefore equation (10) becomes

$$V_{83}=f(8)\frac{A_{(8,3)}k_5[H][O_3]}{L(8)} \qquad (11)$$

Thus the hydrogen concentration can be expressed as

$$[H]=\frac{V_{83}}{f(8)k_5[O_3]}\left[\frac{A(8)}{A(8,3)}+[O_2]\frac{k_{O2}(8)+k_{N2}(8)R}{A(8,3)}\right] \qquad (12)$$

where R represents $[N_2]/[O_2]$.

In the case of the collisional cascade model, using equations (8) and (9), the expression for [H] becomes

$$[H]=\frac{V_{83}}{k_5[O_3]}\left[\frac{A(8)}{A(8,3)}+[O_2]\frac{k_{O2}(8)+k_{N2}(8)R}{A(8,3)}\right]\times\left[f(8)+\frac{f(9)[O_2]}{\frac{A(9)}{k_{O2}(9)}+[O_2]}\right]^{-1} \qquad (13)$$

Again, following *McDade et al.* [1987], the term f(9)A(9,8)/L(9) in the second bracket was neglected. It is also assumed that the quenching factor $k_{N2}(9)$ is much smaller than $k_{O2}(9)$ in the second bracket. From recent laboratory work [*Finlayson-Pitts and Kleindienst*, 1981; *Chalamala and Copeland*, 1993] the former should be less than 5% of the latter.

In addition to the two quenching schemes, sudden death and collisional cascade, two different transition probabilities were used in the present calculation, in order to compare their effect on the resultant profiles. The probabilities used were those of *Murphy* [1971] and *Turnbull and Lowe* [1989]. The quenching factors used were those given by *McDade et al.*[1987] , that is, $\{k_{O2}(8) + k_{N2}(8)R\}/A(8,3)$ equal to 2.0 x 10^{-11} for the sudden death model and 3.3 x 10^{-11} for the collisional cascade model. The cascade quenching factor $A(9)/k_{O2}(9)$ was obtained using the *Finlayson-Pitts and Kleindienst* [1981] quenching coefficient $k_{O2}(9)$ = 1 x 10^{-11} cm^{-3}, recalculated using a new transition probability A(9,3) given by *Turnbull and Lowe* [1989]. These values are listed in Table 2. *Chalamala and Copeland* [1993] have recently reported a direct measurement of $k_{O2}(9)$, giving 1.7 x $10^{-11}cm^{-3}$, which is slightly larger than the value given by *Finlayson-Pitts and Kleindienst* [1981]. The difference in the final value in equation (13) is small, however, as mentioned below.

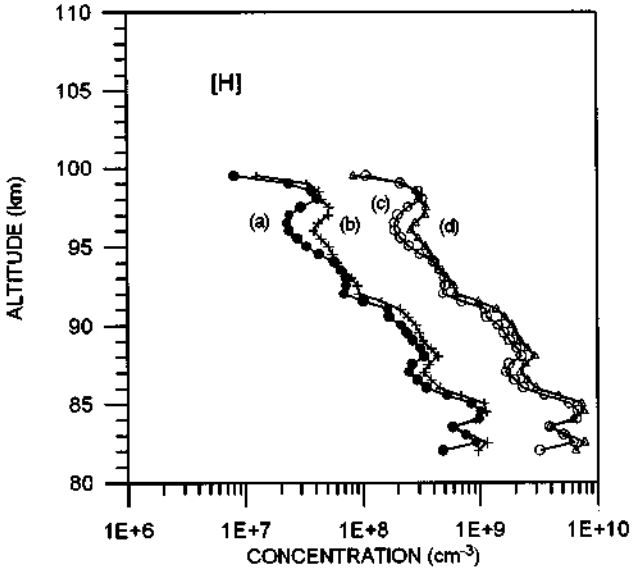

Figure 5 Inferred hydrogen concentrations: (a) using [O] obtained from the O_2 atmospheric (0,0) band emission and $[O_3]$ for α = 0.1; (b) using the OH (8,3) volume emission rate, assuming collisional cascade quenching with *Turnbull and Lowe's* [1989] transition probabilities and $[O_3]$ for α = 0.1; (c) same as Figure 5a but with α = 0.67; (d) same as Figure 5b but with α = 0.67.

The calculated hydrogen profiles are shown in Figure 5, as curves b and d. Only the cases for collisional cascade, equation (13), with the transition probabilities of *Turnbull and Lowe* [1989] are shown. Curve b corresponds to the [H] profile using the ozone profile derived with $\alpha = 0.1$ and curve d corresponds to the case of $\alpha = 0.67$. Between the sudden death and cascade models, it is found that there is a small difference in [H], about 20% at 85 km altitude. Using the same quenching scheme, on the other hand, changing the transition probabilities from those of *Turnbull and Lowe* [1989] to those of *Murphy* [1971], the [H] values increase by about 35%. If the *Chalamala and Copeland* [1993] $k_{O2}(9)$ value were used, the resultant [H] in curve b would increase by around 10%. These variations are, however, much smaller than those resulting from the uncertainty in the fraction α, that is, between curves b and d.

It will be noted that the curves a and b are fairly close to each other, as are curves c and d, showing that the two ways of calculating the hydrogen concentration, one based on equation (7) and the other based on equation (13), are mutually consistent, despite uncertainties such as the unknown quenching scheme in equation (13). This fact supports the results of recent studies of the oxygen-hydrogen-related production and quenching schemes and the relevant reaction rates studied by *McDade et al.* [1986a, 1987].

6. Discussion and Conclusions

In the present study, it was not possible to use both upleg and downleg data because the forward looking OH(8,3) photometer malfunctioned during the upleg. To obtain accurate NaD volume emission rates, it is essential to have the OH(8,2) profile, which in turn must be estimated from the observed OH(8,3) profile. The ozone profile therefore was inferred from the downleg NaD emission profile and the Na density observed by the ground-based lidar at the rocket launching site about 300 km away. This horizontal separation between the Na and the NaD profiles is obviously a potential source of error. As described in section 4, *Clemesha et al.* [1993] presented a NaD profile based on the upleg data. Although this profile is not identical to that which we show in Figure 1, the differences are minor. In particular, both profiles show a rapid rise in intensity at about 85 km and a sharp cutoff above 98 km. The similarity between these two profiles lends confidence to our assumption that the ozone can be derived from the ratio of two profiles obtained at locations separated by 300 km. It may also be relevant that upleg and downleg OI 557.7 nm emission profiles were found to be similar [*Melo et al.* 1995].

Concerning the validity of using the Na-O_3 chemistry to infer the ozone concentration, *Clemesha et al.* [1993] pointed out that the close similarity between the measured Na and the NaD profiles implies an ozone concentration almost independent of height. The unexpected nature of this result led *Clemesha et al.* [1993] to question the validity of the Chapman mechanism. On the other hand, the Chapman mechanism appears to be well established, and no viable alternative has been presented to date. In the present work we assume that the Chapman mechanism is correct in order to derive the ozone concentration. This appears to be a reasonable assumption unless and until further contrary evidence should arise.

Our derived ozone profile shows a wide peak at around 95 km. Recent SME satellite observations [*Thomas*, 1990b] show a secondary ozone peak at around 85 km, as do the model results published by *Allen et al.* [1984], but it should be remembered that the SME data are for daytime conditions. Very few observations have been carried out during the night. In Figure 6 are shown two nighttime rocket measurements, made by *Vaughan* [1982] and *Ulwick et al.* [1987], respectively, and a model profile by *Allen et al.* [1984]. Our present results, (curve d) are based on the assumption of $\alpha = 0.1$. The three rocket measurements are in fairly good agreement. Curve b, the profile presented by *Vaughan* [1982], shows a wide peak at around 90 to 95 km, fairly similar to our profile.

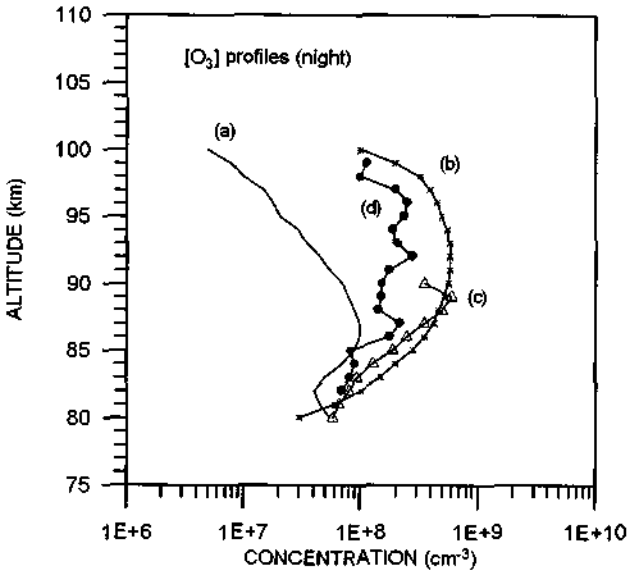

Figure 6 Observed and model [O_3] profiles (nighttime): (a) *Allen et al.* [1984] (model); (b) *Vaughan* [1982] (observation); (c) *Ulwick et al.* [1987] (observation); (d) present results.

As has already been pointed out, [O_3] and [H] in the present work are highly dependent on the branching ratio α of the NaO + O $\rightarrow$ Na(^{2}P) + O_2 reaction. From the airglow data it is difficult to evaluate the range of uncertainty from 0.1 to 0.67. However, it should be pointed out that the O_3 concentration of 2 to 3 x 10^7 cm^{-3}, obtained in the case of $\alpha = 0.67$ (case b of Figure 3), is definitively lower than that suggested by any other measurements. The concentration derived using $\alpha = 0.1$ (case a) is more in keeping with that expected. It should also be mentioned that according to J. M. Plane (private communication, 1994), the higher value of α is unlikely on the basis of energy disposal considerations in exothermic reactions. We conclude that the hydrogen and ozone profiles derived on the basis of $\alpha = 0.1$ are the most likely.

Although [O_3] and [H] in the present work depend crucially on the branching ratio adopted for equation (3), even with the lowest value adopted, the peak concentration of hydrogen at around 85 km is of the order of 10^9 cm^{-3}, which is larger than anything we have seen in the literature. To compare the present results with other data, in Figure 7 the observed distribution is plotted together with a number of published model profiles. The present results shown in the figure are based on the assumptions of a branching ratio $\alpha = 0.1$ and the OH collisional cascade model with the *Turnbull and Lowe* [1989] transition probabilities. The hydrogen profile observed in the present work shows a peak at around 85 km. A direct [H] measurement by resonance lamp technique has been reported by *Sharp and Kita* [1987]. *Ulwick et al.* [1987] have inferred both [O_3] and [H] from the MAP/WINE rocket data. They

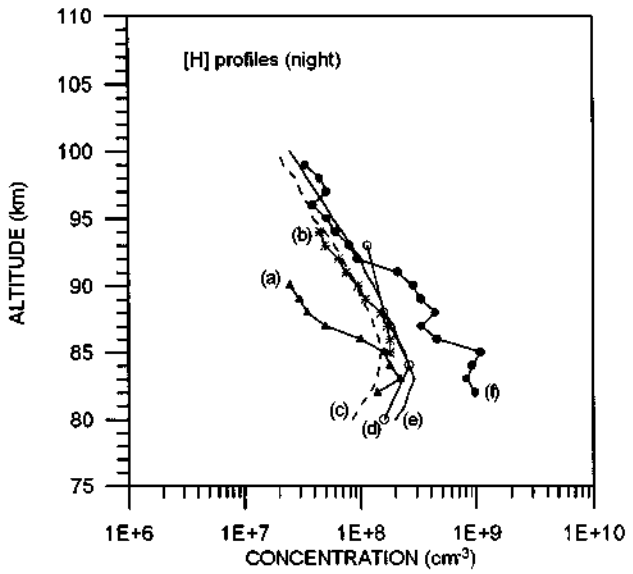

Figure 7 Observed and model [H] profiles (nighttime): (a) *Ulwick et al.* [1987] (observation); (b) *Adler-Golden et al.* [1992] (observation); (c) *Sharp and Kita* [1987] (observation); (d) *Thomas* [1990a] (observation); (e) *Allen et al.* [1984] (model); (f) present results.

determined [O_3] from its 9.6 μm emission and [O] by the resonance lamp technique. The hydrogen concentration was then obtained from the O_3 - H equilibrium condition. On the basis of SME data, *Thomas* [1990a] inferred [O_3] from the $O_2(^1\Delta_g)$ 1.27 μm emission and [H] using the same technique. The [H] values plotted in Figure 7 are for the month of May at the equator and were taken from Table 2 of the Thomas paper. Recently, *Adler-Golden et al.* [1992] inferred [H] from the ozone infrared emission. The only model profile shown is that due to *Allen et al.* [1984]. Although these [H] profiles were obtained at different seasons and latitudes, using different techniques, there is fairly good agreement between them. Number density varies from 2 x 10^8 cm^{-3} at around 82 km to 5 x 10^7 cm^{-3} at 95 km. The present results show good agreement with these profiles above 92 km, but below 90 km, our values are considerably larger than the others, with a discrepancy of about a factor of 4 at 85 km.

The large hydrogen concentration below 90 km merits some discussion. From the SME satellite data [*Thomas*, 1990a], taken in the equatorial region, it can be seen that [H] and [O_3] both show a strong semiannual variation, with maximum [H] and minimum [O_3] in June/July and December/January. The present rocket data were taken at the end of May, the season when [H] would be expected to be moving toward maximum and [O_3] toward minimum. Therefore the present data suggest that when [H] increases during the solstice, the major change occurs below 90 km. This could be the result of greater vertical transport of water vapor, and subsequent photodissociative production of atomic hydrogen, in the equatorial region. The strong semiannual variations observed in the NaD and OI 557.7 nm airglow emission intensities [*Kirchhoff and Takahashi*, 1985; *Takahashi et al.*, 1994], which have been attributed to seasonal variations in the dynamics of the upper atmosphere, are also consistent with this suggestion.

In conclusion, height variations of the nighttime ozone and hydrogen concentrations, derived from simultaneous measurements of the Na density profile and the NaD and OH(8,3) band emissions in the equatorial region, are in general agreement with measurements made at other latitudes. The absolute value of the hydrogen concentration is, however, much larger in the height region below 90 km. Uncertainty in the branching ratio α for the reaction $NaO + O \rightarrow Na(^2P) + O_2$, believed to be responsible to the production of excited sodium, is a limiting factor in the precision of the determination of the absolute values for [O_3] and [H]. A more reliable laboratory determination of the value of α applicable to the NaO + O reaction in the atmosphere is necessary. A direct simultaneous measurement of the vertical profiles of ozone, Na, and the NaD airglow intensity would also help to resolve this question.

Acknowledgments. The present rocket experiment was carried out in cooperation with the Instituto de Aeronáutica e Espaço (IAE) and the Alcântara Launch Center. The authors are grateful to the many people who made this work possible. This work was partially supported by the Conselho Nacional de Desenvolvimento Científico e Tecnológico (CNPq), under contracts 300675/90-9 and 300609/94-9.

References

Adler-Golden, S. M., J. Gruninger, and D. R. Smith, Derivation of atmospheric oxygen and hydrogen profiles from ozone v_3 band emission, *J. Geophys. Res.*, *97*, 19,509-19,518, 1992.

Allen, M., J. I. Lunine, and Y. L. Yung, The vertical distribution of ozone in the mesosphere and lower thermosphere, *J. Geophys. Res.*, *89*, 4841-4872, 1984.

Bates, D. R., and P. C. Ojha, Excitation of the NaD doublet of the nightglow, *Nature*, *286*, 790-791, 1980.

Chalamala, B. R., and R. A. Copeland, Collision dynamics of OH(X, v=9), *J. Chem. Phys.*, *99*, 5807 - 5811, 1993.

Chapman, S., Notes on atmospheric sodium, *Astrophys. J.*, *90*, 309-316, 1939.

Clemesha, B. R., and H. Takahashi, Rocket-borne measurements of horizontal structure in the OH(8,3) and NaD airglow emissions, *Adv. Space Res.*, 17(11), 81-84, 1995.

Clemesha, B. R., H. Takahashi, and Y. Sahai, Vehicle glow observed during a rocket sounding experiment, *Planet. Space Sci.*, *35*, 1367-1372, 1987.

Clemesha, B. R., D. M. Simonich, H. Takahashi, and S. M. L. Melo, A simultaneous measurement of the vertical profiles of sodium nightglow and atomic sodium density in the upper atmosphere, *Geophys. Res. Lett.*, *20*, 1347-1350, 1993.

Clemesha, B. R., D. M. Simonich, H. Takahashi, S. M. L. Melo, and J. M. C. Plane, Experimental evidence for photochemical control of the atmospheric sodium layer, *J. Geophys. Res.*, 100, 18,909-18,916, 1995.

DeMore, W. B., et al., Chemical kinetics and photochemical data for use in stratospheric modeling, in Evaluation 8., *JPL Publ. 87-41*, Jet Propul. Lab., Passadena, California,1987.

Dickinson, P. H. G., W. C. Bain, L. Thomas, E. R. Williams, D. B. Jenkins, and N. D. Twiddy, The determination of the atomic oxygen concentration and associated parameters in the lower ionosphere, *Proc. R. Soc. Lond.*, *369*, 379-408, 1980.

Finlayson-Pitts, B. J., and T. E. Kleindienst, The reaction of hydrogen atoms with ozone as a source of vibrationally excited OH(X) for kinetic studies, *J. Chem. Phys.*, *74*, 5643 - 5658, 1981.

Garcia, R. R., and S. Solomon, The effect of breaking gravity waves on the dynamics and chemical composition of the mesosphere and lower thermosphere, *J. Geophys. Res.*, *90*, 3850-3868, 1985.

Greer, R. G., et al., ETON 1: A data base pertinent to the study of energy transfer in the oxygen nightglow, *Planet. Space Sci.*, *34*, 771-788, 1986.

Grossmann, K. U., et al., Middle atmosphere abundances of water vapor and ozone during MAP/WINE, *J. Atmos. Terr. Phys.*, *49*, 827-841, 1987.

Herschbach, D. R., C. E. Kolb, D. R. Worsnop, and X. Shi, Excitation mechanism of the mesospheric sodium nightglow, *Nature*, *356*, 414-416, 1992.

Johnston, J. E., and A. L. Broadfoot, Midlatitude observations of the

night airglow: Implications to quenching near the mesopause, *J. Geophys. Res., 98*, 21,593-21,603, 1993.

Kirchhoff, V. W., J. H. and H. Takahashi, First sodium nightglow results for Natal, *Planet. Space Sci., 33*, 757-760, 1985.

Kirchhoff, V. W. J. H., B. R. Clemesha, and D. M. Simonich, Seasonal variation of ozone in the mesosphere, *J. Geophys. Res., 86*, 1463-1466, 1981.

Kolb, C. E., and J. B. Elgin, Gas phase chemical kinetics of sodium in the upper atmosphere, *Nature, 263*, 488-490, 1976.

Lin, C. L., and M. T. Leu, Temperature and third body dependence of the rate constant for the reaction $O + O_2 + M \rightarrow O_3 + M$, Int. *J. Chem. Kinet., 14*, 417, 1982.

McDade, I. C., and E. J. Llewellyn, Mesospheric oxygen atom densities inferred from nighttime OH Meinel band emission rates, *Planet. Space Sci., 36*, 897-905, 1988.

McDade, I. C., D. P. Murtagh, R. G. H. Greer, P. H. G. Dickinson, G. Witt, J. Stegman, E. J. Llewellyn, L. Thomas, and D. B. Jenkins, ETON 2: Quenching parameters for the proposed precursors of $O_2(b^1\Sigma_g^+)$ and $O(^1S)$ 557.7 nm in the terrestrial nightglow, *Planet. Space Sci., 34*, 789, 1986a.

McDade, I. C., E. J. Llewellyn, R. G. H. Greer, and D. P. Murtagh, ETON 3: Altitude profiles of the nightglow continuum at green and near infrared wavelengths, *Planet. Space Sci., 34*, 801-810, 1986b.

McDade, I. C., E. J. Llewellyn, D. P. Murtagh, and R. G. H. Greer, ETON 5: Simultaneous rocket measurements of the OH Meinel (8,3) band and $\Delta v = 2$ sequence in the nightglow, *Planet. Space Sci., 35*, 1137, 1987.

Melo, S. M. L., H. Takahashi, B. R. Clemesha, P. P. Batista, and D. M. Simonich, Atomic oxygen concentrations from rocket airglow observations in the equatorial region, *J. Atmos. Terr. Phys.*, in press, 1995.

Murphy, R. E., Infrared emission of OH in the fundamental and first overtone bands, *J. Chem. Phys., 54*, 4852-4859, 1971.

Murtagh, D. P., R. G. H. Greer, I. C. McDade, E. J. Llewellyn and M. Bantle, Representative Volume Emission Profiles from Rocket Photometer Data, *Ann. Geophys., 2*, 467-474, 1984.

Murtagh, D. P., G. Witt, J. Stegman, I. C. McDade, E. J. Llewellyn, F. Harris, and R. G. H. Greer, An assessment of proposed $O(^1S)$ and $O_2(b^1\Sigma_g^+)$ nightglow excitation parameters, *Planet. Space Sci., 38*, 43-53, 1990.

Ohoyama, H., T. Kasai, Y. Yoshimura, H. Kimura, and K. Kuwata, Initial distribution of vibration of the OH radicals produced in the $H + O_3 = OH(X^2\Pi) + O_2$ reaction chemiluminescence by a crossed beam technique, *Chem.Phys. Lett., 118*, 263-267, 1985.

Plane, J. M. C., and D. Husain, Determination of the absolute rate constant for the reaction $NaO + O \rightarrow Na + O_2$ by time-resolved atomic chemiluminescence at lambda = 589 nm [$Na(3\ ^2P_1) \rightarrow Na(3\ ^2S_{1/2}) + h\nu$], *J. Chem. Soc., 82*, 2047-2052, 1986.

Plane, J. M. C., C. F. Nien, M. R. Allen, and M. Helmer, A kinetic investigation of the reactions $Na + O_3$ and $NaO + O_3$ over the temperature range 207-377 K, *J. Phys. Chem., 97*, 4459-4467, 1993.

Sharp, W. E., and D. Kita, In situ measurement of atomic hydrogen in the upper mesosphere, *J. Geophys. Res., 92*, 4319-4324, 1987.

Takahashi, H., and P. P. Batista, Simultaneous measurements of OH(9,4), (8,3), (7,2), (6,2) and (5,1) bands in the airglow, *J. Geophys. Res.*, 86, 5632, 1981.

Takahashi, H., B. R. Clemesha, Y. Sahai, P. Batista, and D. M. Simonich, Seasonal variations of mesospheric hydrogen and ozone concentrations derived from ground-based airglow and lidar observations, *J. Geophys. Res., 97*, 5987, 1992.

Takahashi, H., B. R. Clemesha, and P. P. Batista, Predominant semi-annual oscillation of the upper mesospheric airglow intensities and temperatures in the equatorial region, *J. Atmos. Terr. Phys., 57*, 407-414, 1994.

Thomas, R. J., Atomic hydrogen and atomic oxygen density in the mesopause region: Global and seasonal variations deduced from Solar Mesosphere Explorer near-infrared emissions, *J. Geophys. Res., 95*, 16,457-16,476, 1990a.

Thomas, R. J., Seasonal ozone variations in the upper mesosphere, *J. Geophys. Res., 95*, 7395-7401, 1990b.

Thomas, R. J., and R. . Young, Measurements of atomic oxygen and relaated airglow in the lower thermosphere, *J. Geophys. Res., 86*, 7389-7393, 1981.

Turnbull, D. N., and R. P. Lowe, New hydroxyl transition probabilities and their importance in airglow studies, *Planet. Space Sci., 37*, 723-738, 1989.

Ulwick, J. C., K. D. Baker, D. J. Baker, A. J. Steed, P. J. W.R., K. Grossmann, and H. G. Bruckelmann, Mesospheric minor species determinations from rocket and ground-based i.r. measurements, *J. Atmos. Terr. Phys., 49*, 855-862, 1987.

Vaughan, G., Diurnal variation of mesospheric ozone, *Nature, 296*, 133-135, 1982.

Worsnop, D. R., M. S. Zahniser, and C. E. Kolb, Low-temperature absolute rate constants for the reaction of atomic sodium with ozone and nitrous oxide, *J. Phys. Chem., 95*, 3960-3964, 1991.

B. R. Clemesha, S. M. L. Melo, D. M. Simonich, and H. Takahashi, INPE, C.P. 515, São.José. dos Campos, São Paulo 12201-970, Brazil. (e-mail: inpedaa@eu.ansp.br)

J. Stegman and G. Witt, Meteorology Department, Stockholm University, S 10691 Stockholm, Sweden

(Received June 28, 1994; revised July 13, 1995;
accepted September 19, 1995.)

JOURNAL OF GEOPHYSICAL RESEARCH, VOL. 101, NO. D2, PAGES 4033–4040, FEBRUARY 20, 1996

Atomic hydrogen and ozone concentrations derived from simultaneous lidar and rocket airglow measurements in the equatorial region

Hisao Takahashi, Stella. M. L. Melo, B. R. Clemesha, and D. M. Simonich
Instituto Nacional de Pesquisas Espaciais, INPE, São José dos Campos, Brazil

J. Stegman and G. Witt
Department of Meteorology, Stockholm University, Sweden

Abstract. Nighttime atomic hydrogen and ozone concentrations are derived from simultaneous measurements of the vertical profiles of upper mesospheric airglow emissions and atmospheric sodium. The airglow profiles were obtained in a sounding rocket experiment launched from Alcântara (2.5°S, 44.2°W) on May 31, 1992. A lidar operating at the launch site was used to measure sodium at the time of the rocket experiment. A total of 10 airglow photometers, 6 forward looking and 4 side looking, observed the OI 557.7 nm, O_2 Herzberg and O_2 atmospheric (0,0) bands, sodium D lines, OI 630 nm, OH(8,3) band, and the airglow continuum. The simultaneous ground-based sodium lidar and onboard sodium airglow measurements made it possible to derive the ozone concentration at heights between 85 and 100 km. The hydrogen concentrations were then calculated from the O_2 atmospheric (0,0), OH(8,3), and the ozone profiles. The results suggest that the hydrogen concentration varied from 1×10^9 cm^{-3} at 85 km to 1×10^8 cm^{-3} at 100 km, values much higher than those suggested by recent model atmospheres and by some rocket observations at middle and high latitudes. Although the method of obtaining the concentrations of the minor constituents in the upper atmosphere is an indirect optical technique, this is the first time that these concentrations have been measured by rocket in the equatorial region.

1. Introduction

Atomic oxygen, ozone, and atomic hydrogen are the main species that control photochemical processes in the upper mesosphere and the lower thermosphere between 80 and 120 km. To understand the behavior of these species, in terms of day-to-day and seasonal variations, dependence on latitude and height, it is very important to investigate not only the photochemical processes involved but also the dynamical processes that occur in this altitude range. The height profiles are highly dependent on vertical mixing processes and meridional circulation [*Garcia and Solomon*, 1985]. Observation and monitoring of these species, however, is still very limited, owing to the technical difficulties involved.

Atomic oxygen has been measured by the resonance lamp technique on board a rocket [*Dickinson et al.*, 1980]. Several rocket measurements have been carried out using this technique together with oxygen airglow measurements [*Thomas and Young*, 1981; *Greer et al.*, 1986]. Through these experiments, it has been possible to obtain empirical values for the transition probabilities and quenching coefficients required to derive atomic oxygen concentration from airglow emissions [*Murtagh et al.*, 1990]. Today, the oxygen-related airglow emissions are used to calculate the concentration of atomic oxygen, using the OI 557.7 nm and O_2 atmospheric band emissions for the height range 85 to 110 km and hydroxyl band emissions for below 90 km [*McDade and Llewellyn*, 1988].

Daytime ozone concentration can be obtained from measurements of the $O_2(^1\Delta)$ 1.27 μm emission which results from ozone photolysis by solar ultraviolet radiation. During the nighttime, on the other hand, the only direct measurement technique available is to measure the infrared radiation from ozone [*Grossman et al.*, 1987]. The results of indirect measurements, using lidar profiles of sodium density together with airglow measurements of the 589 nm emission, have been presented by *Kirchhoff et al.* [1981], *Takahashi, et al.*, [1992], and *Clemesha et al.* [1993].

Atomic hydrogen is one of the more difficult species to measure directly in the upper atmosphere. Hitherto, using a direct technique, only one rocket measurement has been carried out by *Sharp and Kita* [1987]. Using an indirect technique, *Thomas* [1990a] derived hydrogen concentrations from the ozone density and the OH airglow intensity determined from the SME satellite data. *Takahashi et al.* [1992] used a similar technique to estimate hydrogen using ground-based observations. *Adler-Golden et al.*[1992] measured infrared ozone ν_3 band emissions by rocket and succeeded in deriving O and H atom concentration profiles.

In the present study, ozone concentration is first inferred from profiles of the NaD emission and the Na density, measured by rocket-borne photometers and lidar, respectively.

Paper number 95JD03035.
0148-0227/96/95JD-03035$05.00

Subsequently, hydrogen concentration is calculated in two ways: one from the ozone concentration and the atomic oxygen concentration inferred from the O_2 atmospheric (0,0) band and the other from the ozone concentration and the OH (8,3) emission profile. This is the first combined ground-based and rocket experiment from which it has been possible to estimate nighttime ozone and hydrogen concentrations in the equatorial mesopause region.

2. Experiments

The MULTIFOT payload, which included six forward looking and four side looking airglow photometers and two ionospheric plasma probes, was launched by a SONDA III rocket from the Alcântara Launch Center (2.5°S, 44.2°W), at 2352 Local Standard Time on May 31, 1992. During its 12 min flight the payload reached an altitude of 282 km and traveled a horizontal distance of 398 km.

The purpose of the experiment was to measure the vertical profiles of the O_2 Herzberg, O_2 atmospheric (0,0), and OH(8,3) bands together with the OI 557.7 nm and NaD 589.3 nm emissions between 80 to 120 km in the upper mesosphere and lower thermosphere. A 578 nm forward looking photometer was used to estimate the background airglow continuum. The data used in the present study were from the forward looking NaD 589.3 nm, OH(8,3) 724 nm R branch, and BG 578 nm photometers. The photometer specifications are shown in Table 1.

The photometer spectral and absolute sensitivities were calibrated in the laboratory using a laboratory standard (Eppley 100W) lamp and MgO white diffuser. The photometers included tritium-activated light sources to check their sensitivities during the flight. No changes from the preflight values were detected.

Measurements of the atomic sodium concentration were made using a lidar system installed approximately 5 km from the launch ramp. Information on the lidar measurements and conditions of observation during the flight can be found in the work of *Clemesha et al.* [1993].

3. NaD and OH(8,3) Emission Profiles

During the upleg passage through the emission region the OH(8,3) and O_2 atmospheric (0,0) band photometers suffered strong extraneous noise contamination, which started before the nose cone opened and lasted for about 50 s, after which time it disappeared completely. This made it impossible to reduce the upleg data from these two photometers. However, neither the NaD 589.3 nm photometer nor the BG 578 nm photometer suffered any noise contamination. During the downleg passage, contamination was detected from none of the photometers. This was concluded from the fact that the wideband (10 nm) BG 578 nm photometer showed similar signals during upleg and downleg passages through the emission region and did not show any unexpected variations in intensity. In the present experiment, no obvious light contamination, such as the vehicle glow observed by *Clemesha et al.* [1987], was detected. Although the same type of rocket (SONDA III) was used, the payload configuration was totally different, and the vehicle velocity was much lower. Because of the extraneous upleg signals observed from the infrared photometers, only the downleg data will be used in calculating the volume emission rates used in the present study.

Table 1. Rocket-Borne Photometer Specifications

Photometer	λ, nm	Δλ, nm	PMT	Sensitivity *
O_2 Herzberg	275.0	14.3	EMI 9924	191.0
OI 5577	557.7	1.7	EMI 9924	684.0
BG 578	578.0	11.0	EMI 9924	220.2
NaD 5893	589.0	1.7	EMI 9924	326.9
OH(8,3)	724.2	1.9	EMI 9798	143.9
O_2 atm. (0,0)	762.0	5.7	EMI 9798	43.6

Photometer field of view: 4° (half angle); optical diameter of objective lens: 46 mm; orientation: forward looking (parallel to the rocket axis).

*Counts s^{-1} Rayleigh^{-1}.

To determine the intensity of the NaD (D_1+ D_2) emission, it is necessary to take into account spectral contamination from the OH(8,2) Q branch and the airglow continuum superposed in the filter passband. The contribution of OH(8,2) was calculated using the observed OH(8,3) band intensity with an appropriate instrumental factor and the ratio of the relevant transition probabilities. The continuum contribution in the 589 nm region was estimated by using an appropriate fraction of the continuum intensity observed at 578 nm. The OH(8,2) contribution to the 589.3 nm photometer signal was found to be 21% at the peak of the OH emission layer, and the continuum emission contributed a maximum of 11% at a height of 85 km. The NaD volume emission profile obtained in this way for the downleg is plotted in Figure 1. An incremental straight line fitting technique [*Murtagh et al.*, 1984] with a 4 km fitting length was used to smooth the profile.

Figure 1 also shows the lidar sodium profile. It can be seen that the profiles of airglow volume emission rate (proportional to the concentration of excited sodium) and the Na density (proportional to the density of ground state sodium) are fairly similar, with sharp boundaries both at the bottom and at the top of the layers. In this context it should be remembered that the two profiles refer to regions separated by a horizontal distance of approximately 300 km.

In the case of the OH(8,3) R branch, spectral contamination at 724 nm from the airglow continuum was estimated from the continuum observed at the 578 nm region. To estimate the ratio between the intensities in the 724 nm and 578 nm regions, we used data from the ETON campaign [*McDade et al.*, 1986b], leading to the adoption of a value of 1.33 for $I_{(724)}/I_{(578)}$. This ratio, however, could be height dependent. According to *McDade et al.*[1986b] it could vary from 1.0 to 2.0 between 90 and 100 km. However, the error due to this uncertainty should be negligible in the present study. The contribution of the continuum to the OH(8,3) photometer signal was around 8% of the total output. The uncertainty originating from the continuum subtraction, therefore, should be less than 3%, which is less than the experimental error from other sources. The resulting OH(8,3) emission profile is shown in Figure 2. The peak height is around 87 km with a half-width of approximately 10 km. The observed integrated intensity, 550 Rayleigh, is somewhat higher than expected. A ground-based photometer at the launch site measured an OH(9,4) band intensity of about 700 R. On the basis of the intensity ratio of 1.6 for $I_{(9,4)}/I_{(8,3)}$, obtained by *Takahashi and Batista* [1981], the OH(8,3) intensity should be around 440 R. However recent ground-based observation carried out by *Johnston and Broadfoot* [1993] showed similar intensity levels for the OH(9,4) and OH(8,3) bands. If this is correct, our present results, suggesting an intensity ratio of 1.3, are not surprising.

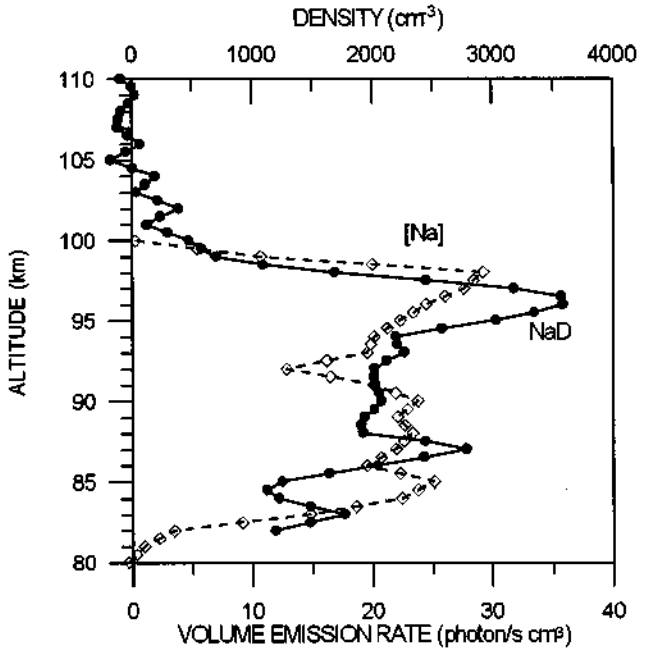

Figure 1 NaD volume emission rate measured by rocket and the Na atom concentrations measured by ground-based lidar, both for the Alcântara launch site, May 31, 1992.

It could be that latitudinal or local differences in photochemical equilibrium lead to differences in the OH vibrational distribution.

One of the side looking photometers in the present payload also measured the OH(8,3) band intensity. Since the payload rotation caused the side looking photometers to scan the emission layers, these instruments provided information on horizontal variations in emission intensity. An analysis of the data from the side looking photometers [*Clemesha and Takahashi*, 1995] has shown variations by nearly a factor of 2 occurring over a horizontal distance of little more than 100 km, in the region of the downleg passage of the payload through the emitting region. For this reason it cannot be ruled out that the relatively high OH(8,3) integrated intensity was due to local variations in the emission intensities. It should be pointed out, however, that the OI 557.7 photometer showed significant differences in neither the integrated intensities nor the emission rate profiles between upleg and downleg.

4. Ozone Concentration

It is generally accepted that the sodium nightglow emission results mainly from the Chapman mechanism [*Chapman*, 1939],

$$Na + O_3 \rightarrow NaO + O_2 \quad k_1 \qquad (1)$$

$$NaO + O \rightarrow Na(^2P) + O_2 \quad \alpha k_2 \qquad (2)$$

It is conceivable that other mechanisms exist for the production of $Na(^2P)$. However, there is no reason to believe that any of these make a significant contribution to the NaD airglow emission. The NaD volume emission rate is directly related to the rate of production of $Na(^2P)$ via equation (2), and since the processes of oxidation (1) and reduction (2) are very rapid and in quasi-equilibrium, the NaD emission rate is equal to

$$V_{(NaD)} = k_1 \alpha [Na][O_3] \qquad (3)$$

where k_1 and k_2 are chemical reaction rates and the branching ratio, α, is the fraction of Na atoms produced in the (^2P) state. The brackets indicate number densities. The radiative lifetime of $Na(^2P)$ is so short (nanoseconds) that there can be no significant quenching. Therefore given the atomic sodium and NaD emission profiles, and values for k_1 and α, the ozone concentration (hereinafter $[O_3]$) can be determined.

There is some consensus of opinion concerning the absolute value of k_1 [*Worsnop*, 1991, *Plane et al.*, 1993]. However, this is not true in case of the branching ratio α. Laboratory measurements by *Plane and Husain* [1986] have indicated values less than 0.01, and *Bates and Ohja* [1980] suggested a value of around 0.3. Recent theoretical work by *Herschbach et al.*[1992] suggests a much higher value, around 0.67. This value is based on the possibility that NaO is produced in an electronically excited state and that the excess energy leads to a higher yield for excited Na than is observed in laboratory measurements. On the other hand, there is no experimental evidence for this hypothesis. It is more plausible that the excess chemical energy in reaction (2) would go to a newly formed O_2 bond. Recent work by *Plane et al.*[1993] and *Clemesha et al.*[1995] suggests that the fraction should be much smaller than that suggested by Herschbach and that it should be around 0.1. In view of this uncertainty, we have calculated ozone concentrations for what appear to be reasonable limiting values of 0.1 and 0.67. The adopted reaction rates and other parameters are listed in Table 2. The ozone profiles calculated in this manner are shown in Figure 3.

As expected from the similarity between the height profiles of NaD and Na shown in Figure 1, the calculated O_3 profiles in Figure 3 do not show the clear peak seen in model atmospheres [e.g., *Allen et al.*,1984]. In the case of α=0.1, the concentration varies from $1x10^8$ cm^{-3} at around 85 km to $2.5x10^8$ cm^{-3} at around 95 km.

In the paper by *Clemesha et al.* [1993] the O_3 profile was inferred from the same rocket experiment but using the upleg NaD profile and a value of 0.67 for α. In the absence of upleg

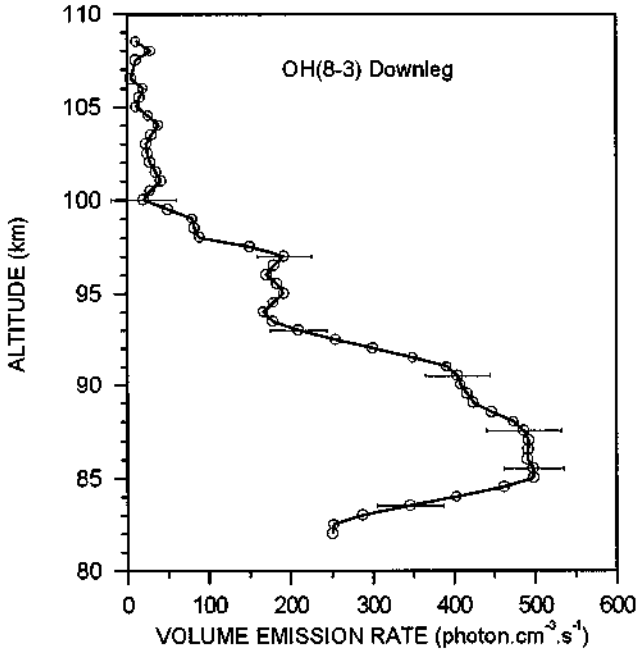

Figure 2 OH (8,3) band volume emission rate observed from Alcântara, May 31, 1992.

Table 2. Reactions and Adopted Parameters

Reaction	Rate	Reference
(1) $Na + O_3 \rightarrow NaO + O_2$	$k_1 = 1.6 \times 10^{-9} \exp(-195/T)$	Worsnop et al.[1991]
(2) $NaO + O \rightarrow Na(^2P) + O_2$	$\alpha \leq 0.1$	Kolb and Elgin[1976]
	$\alpha = 0.3$	Bates and Ojha[1980]
	$\alpha = 0.67$	Herschbach et al.[1992]
(4) $O + O_2 + M \rightarrow O_3 + M$	$k_{4(N2)} = 5.7\times10^{-34}(T/300)^{-2.62}$	Lin and Leu [1982]
	$k_{4(N2)} = 5.7\times10^{-34}(T/300)^{-2.62}$	Lin and Leu [1982]
(5) $O_3 + H \rightarrow OH^*(v) + O_2$	$k_5 = 1.4\times10^{-10} \exp(-470/T)$	DeMore et al. [1987]
(6) $O_3 + O \rightarrow O_2 + O_2$	$k_6 = 8.0\times10^{-12} \exp(-2060/T)$	DeMore et al. [1987]
$A(8)/A(8,3) = 320$		Murphy[1971]
$A(8)/A(8,3) = 118$		Turnbull and Lowe [1989]
$f(9) = 0.32$		Ohyama et al. [1985]
$f(8) = 0.29$		Ohyama et al. [1985]
$A(9)/k_{O2}(9) = 5.8\times10^{12}$		see text

data from the forward looking 724.2 nm photometer, the contribution of OH(8,2) to the 589.3 nm photometer signal was estimated from the OH(8,3) intensity measured by one of the side looking photometers. In the presence of strong horizontal gradients this could result in an error in estimating the contribution of the OH(8,2) emission. In the present work we will use the OH(8,3) band intensity, together with the ozone profile, to estimate the hydrogen concentration. For this reason it was preferred to use the downleg NaD and OH profiles, both derived from forward looking photometers. Although this means that the ozone is derived from Na and NaD profiles measured at locations separated by about 300 km, as discussed later, we do not believe that this introduces an important error. It should be noted that the ozone distribution derived in the present analysis, profile b in Figure 3, does not differ greatly from that presented in the earlier paper.

5. Hydrogen Concentration

Although the photochemistry of oxygen and hydrogen in the upper mesosphere and lower thermosphere is complex, the equilibrium between atomic hydrogen and ozone can be expressed simply. The main ozone production process is

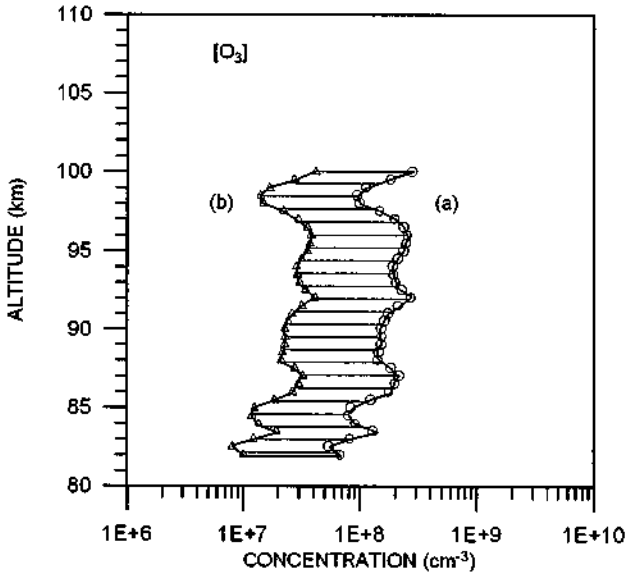

Figure 3 Inferred ozone concentrations for (a) $\alpha = 0.1$; (b) $\alpha = 0.67$.

$$O + O_2 + M \rightarrow O_3 + M \quad k_4 \qquad (4)$$

There are two ozone loss processes:

$$O_3 + H \rightarrow OH^*(v) + O_2 \quad k_5 \qquad (5)$$

which is the main loss process, producing vibrationally excited OH, and

$$O_3 + O \rightarrow O_2 + O_2 \quad k_6 \qquad (6)$$

which is slow compared to reaction (5) but becomes non negligible above 95 km.

From the photochemical equilibrium of ozone in equations (4), (5), and (6) the hydrogen concentration (here in after [H]) can be calculated as

$$[H] = \frac{k_4[O][O_2][M]}{k_5[O_3]} - \frac{k_6}{k_5}[O] \qquad (7)$$

Therefore if [O], $[O_2]$, $[O_3]$, and [M] are given, [H] can be calculated.

In the present work, [O] was derived from the O_2 atmospheric (0,0) band volume emission rate profile observed by the same payload. The details of how this was done are presented by *Melo et al.*[1995]. The resulting atomic oxygen profile is shown in Figure 4. Also shown in Figure 4, for comparison, is an [O] profile computed from the MSIS model for the appropriate input conditions. It is noted that the present [O] profile is in some agreement with the model, not showing any anomalous feature. Temperature and the O_2 and N_2 profiles were taken from the CIRA-86 model for heights up to 90 km and the MSIS model for greater heights. The CIRA and MSIS temperatures were adjusted to agree with the OH rotational temperature measured by the ground-based photometer at the time of the launch, and the major constituent profiles were adjusted to maintain hydrostatic equilibrium. The results for the hydrogen concentrations are shown in Figure 5. Curve a in this figure corresponds to the case of ozone formation with the fraction $\alpha = 0.1$. Curve c corresponds to $\alpha = 0.67$.

The hydrogen concentration can also be calculated by using $[O_3]$ and the observed OH(8,3) band intensity. Following *McDade et al.* [1987], the OH(8,3) band volume emission rate, V_{83}, is given by

$$V_{83} = \frac{A_{(8,3)}k_5[H][O_3]}{L(8)}\left[f(8) + f(9)\frac{A_{(9,8)} + \sum_Q k_Q(9,8)[Q]}{L(9)}\right] \qquad (8)$$

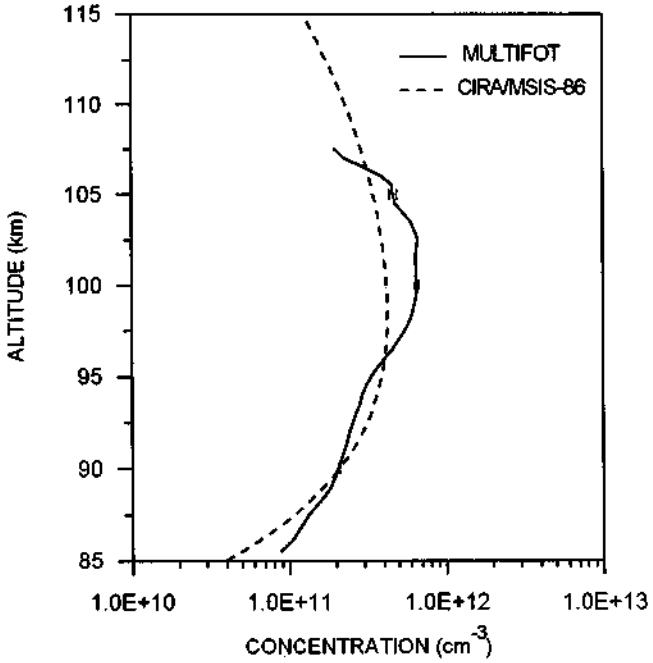

Figure 4 Atomic oxygen concentrations obtained from the observed O_2 atmospheric (0,0) band volume emission rate, compared with an [O] profile from the MSIS model.

where f(8) and f(9) represent the fractions of OH excited into the vibrational levels 8 and 9, respectively, and L(8) and L(9) represent the total losses from these levels; that is,

$$L(v)=A(v)+\Sigma_Q k_Q(v)[Q] \qquad (9)$$

where A(v) is the vibrational transition probability of level v, and Q is the quenching agent, mainly N_2 and O_2.

For the vibrationally excited OH quenching process, *McDade et al.* [1987] considered two different schemes, sudden death and collisional cascade. The former assumes that any collisional deactivation of the vibrationally excited OH causes its total energy loss immediately, i.e., from v to v = 0. On the other hand, the latter assumes that the collisional deactivation causes only one step vibrational cascading, i.e., from v to v-1. Therefore in the case of the sudden death model, the term "$k_Q(9,8)$" in equation (8) is equal to zero,

$$V_{83}=\frac{A_{(8,3)}k_5[H][O_3]}{L(8)}\left[f(8)+f(9)\frac{A_{(9,8)}}{L(9)}\right] \qquad (10)$$

As pointed out by *McDade et al.* [1987], the term f(9)A(9,8)/L(9) is considerably smaller than f(8), so it can be neglected. Therefore equation (10) becomes

$$V_{83}=f(8)\frac{A_{(8,3)}k_5[H][O_3]}{L(8)} \qquad (11)$$

Thus the hydrogen concentration can be expressed as

$$[H]=\frac{V_{83}}{f(8)k_5[O_3]}\left[\frac{A(8)}{A(8,3)}+[O_2]\frac{k_{O2}(8)+k_{N2}(8)R}{A(8,3)}\right] \qquad (12)$$

where R represents $[N_2]/[O_2]$.

In the case of the collisional cascade model, using equations (8) and (9), the expression for [H] becomes

$$[H]=\frac{V_{83}}{k_5[O_3]}\left[\frac{A(8)}{A(8,3)}+[O_2]\frac{k_{O2}(8)+k_{N2}(8)R}{A(8,3)}\right]\times\left[f(8)+\frac{f(9)[O_2]}{\frac{A(9)}{k_{O2}(9)}+[O_2]}\right]^{-1} \qquad (13)$$

Again, following *McDade et al.* [1987], the term f(9)A(9,8)/L(9) in the second bracket was neglected. It is also assumed that the quenching factor $k_{N2}(9)$ is much smaller than $k_{O2}(9)$ in the second bracket. From recent laboratory work [*Finlayson-Pitts and Kleindienst*, 1981; *Chalamala and Copeland*, 1993] the former should be less than 5% of the latter.

In addition to the two quenching schemes, sudden death and collisional cascade, two different transition probabilities were used in the present calculation, in order to compare their effect on the resultant profiles. The probabilities used were those of *Murphy* [1971] and *Turnbull and Lowe* [1989]. The quenching factors used were those given by *McDade et al.*[1987] , that is, $\{k_{O2}(8) + k_{N2}(8)R\}/A(8,3)$ equal to 2.0 x 10^{-11} for the sudden death model and 3.3 x 10^{-11} for the collisional cascade model. The cascade quenching factor $A(9)/k_{O2}(9)$ was obtained using the *Finlayson-Pitts and Kleindienst* [1981] quenching coefficient $k_{O2}(9)$ = 1 x 10^{-11} cm^{-3}, recalculated using a new transition probability A(9,3) given by *Turnbull and Lowe* [1989]. These values are listed in Table 2. *Chalamala and Copeland* [1993] have recently reported a direct measurement of $k_{O2}(9)$, giving 1.7 x $10^{-11}$$cm^{-3}$, which is slightly larger than the value given by *Finlayson-Pitts and Kleindienst* [1981]. The difference in the final value in equation (13) is small, however, as mentioned below.

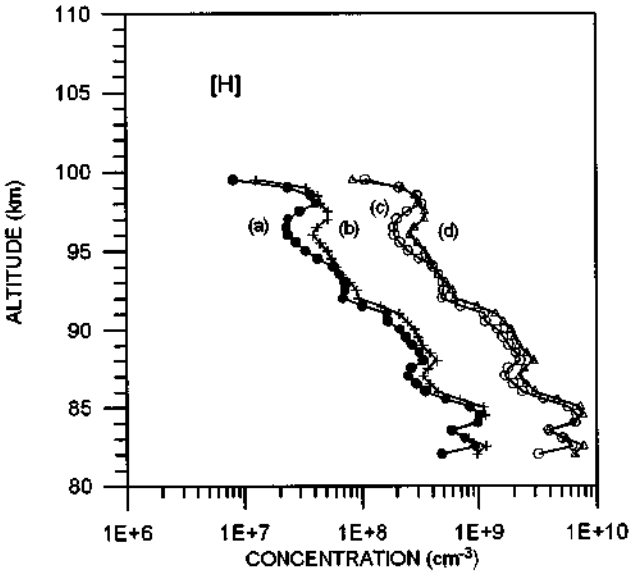

Figure 5 Inferred hydrogen concentrations: (a) using [O] obtained from the O_2 atmospheric (0,0) band emission and $[O_3]$ for α = 0.1; (b) using the OH (8,3) volume emission rate, assuming collisional cascade quenching with *Turnbull and Lowe's* [1989] transition probabilities and $[O_3]$ for α = 0.1; (c) same as Figure 5a but with α = 0.67; (d) same as Figure 5b but with α = 0.67.

The calculated hydrogen profiles are shown in Figure 5, as curves b and d. Only the cases for collisional cascade, equation (13), with the transition probabilities of *Turnbull and Lowe* [1989] are shown. Curve b corresponds to the [H] profile using the ozone profile derived with $\alpha = 0.1$ and curve d corresponds to the case of $\alpha = 0.67$. Between the sudden death and cascade models, it is found that there is a small difference in [H], about 20% at 85 km altitude. Using the same quenching scheme, on the other hand, changing the transition probabilities from those of *Turnbull and Lowe* [1989] to those of *Murphy* [1971], the [H] values increase by about 35%. If the *Chalamala and Copeland* [1993] $k_{O2}(9)$ value were used, the resultant [H] in curve b would increase by around 10%. These variations are, however, much smaller than those resulting from the uncertainty in the fraction α, that is, between curves b and d.

It will be noted that the curves a and b are fairly close to each other, as are curves c and d, showing that the two ways of calculating the hydrogen concentration, one based on equation (7) and the other based on equation (13), are mutually consistent, despite uncertainties such as the unknown quenching scheme in equation (13). This fact supports the results of recent studies of the oxygen-hydrogen-related production and quenching schemes and the relevant reaction rates studied by *McDade et al.* [1986a, 1987].

6. Discussion and Conclusions

In the present study, it was not possible to use both upleg and downleg data because the forward looking OH(8,3) photometer malfunctioned during the upleg. To obtain accurate NaD volume emission rates, it is essential to have the OH(8,2) profile, which in turn must be estimated from the observed OH(8,3) profile. The ozone profile therefore was inferred from the downleg NaD emission profile and the Na density observed by the ground-based lidar at the rocket launching site about 300 km away. This horizontal separation between the Na and the NaD profiles is obviously a potential source of error. As described in section 4, *Clemesha et al.* [1993] presented a NaD profile based on the upleg data. Although this profile is not identical to that which we show in Figure 1, the differences are minor. In particular, both profiles show a rapid rise in intensity at about 85 km and a sharp cutoff above 98 km. The similarity between these two profiles lends confidence to our assumption that the ozone can be derived from the ratio of two profiles obtained at locations separated by 300 km. It may also be relevant that upleg and downleg OI 557.7 nm emission profiles were found to be similar [*Melo et al.* 1995].

Concerning the validity of using the Na-O_3 chemistry to infer the ozone concentration, *Clemesha et al.* [1993] pointed out that the close similarity between the measured Na and the NaD profiles implies an ozone concentration almost independent of height. The unexpected nature of this result led *Clemesha et al.* [1993] to question the validity of the Chapman mechanism. On the other hand, the Chapman mechanism appears to be well established, and no viable alternative has been presented to date. In the present work we assume that the Chapman mechanism is correct in order to derive the ozone concentration. This appears to be a reasonable assumption unless and until further contrary evidence should arise.

Our derived ozone profile shows a wide peak at around 95 km. Recent SME satellite observations [*Thomas*, 1990b] show a secondary ozone peak at around 85 km, as do the model results published by *Allen et al.* [1984], but it should be

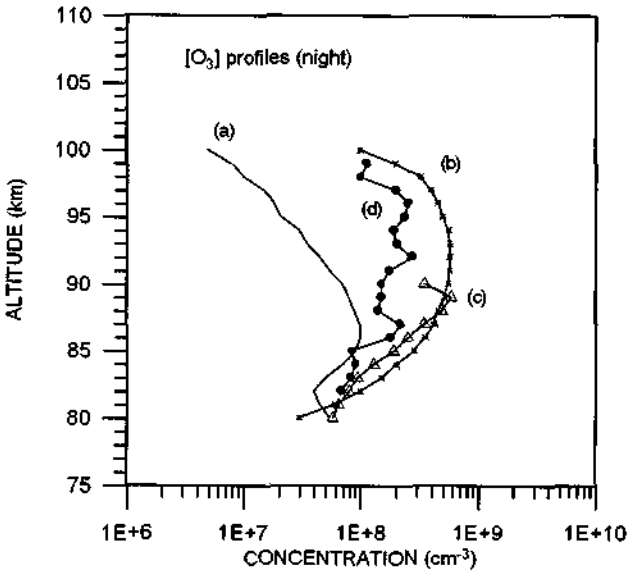

Figure 6 Observed and model [O_3] profiles (nighttime): (a) *Allen et al.* [1984] (model); (b) *Vaughan* [1982] (observation); (c) *Ulwick et al.* [1987] (observation); (d) present results.

remembered that the SME data are for daytime conditions. Very few observations have been carried out during the night. In Figure 6 are shown two nighttime rocket measurements, made by *Vaughan* [1982] and *Ulwick et al.* [1987], respectively, and a model profile by *Allen et al.* [1984]. Our present results, (curve d) are based on the assumption of $\alpha = 0.1$. The three rocket measurements are in fairly good agreement. Curve b, the profile presented by *Vaughan* [1982], shows a wide peak at around 90 to 95 km, fairly similar to our profile.

As has already been pointed out, [O_3] and [H] in the present work are highly dependent on the branching ratio α of the NaO + O $\rightarrow$ Na(^{2}P) + O_2 reaction. From the airglow data it is difficult to evaluate the range of uncertainty from 0.1 to 0.67. However, it should be pointed out that the O_3 concentration of 2 to 3 x 10^7 cm^{-3}, obtained in the case of $\alpha = 0.67$ (case b of Figure 3), is definitively lower than that suggested by any other measurements. The concentration derived using $\alpha = 0.1$ (case a) is more in keeping with that expected. It should also be mentioned that according to J. M. Plane (private communication, 1994), the higher value of α is unlikely on the basis of energy disposal considerations in exothermic reactions. We conclude that the hydrogen and ozone profiles derived on the basis of $\alpha = 0.1$ are the most likely.

Although [O_3] and [H] in the present work depend crucially on the branching ratio adopted for equation (3), even with the lowest value adopted, the peak concentration of hydrogen at around 85 km is of the order of 10^9 cm^{-3}, which is larger than anything we have seen in the literature. To compare the present results with other data, in Figure 7 the observed distribution is plotted together with a number of published model profiles. The present results shown in the figure are based on the assumptions of a branching ratio $\alpha = 0.1$ and the OH collisional cascade model with the *Turnbull and Lowe* [1989] transition probabilities. The hydrogen profile observed in the present work shows a peak at around 85 km. A direct [H] measurement by resonance lamp technique has been reported by *Sharp and Kita* [1987]. *Ulwick et al.* [1987] have inferred both [O_3] and [H] from the MAP/WINE rocket data. They

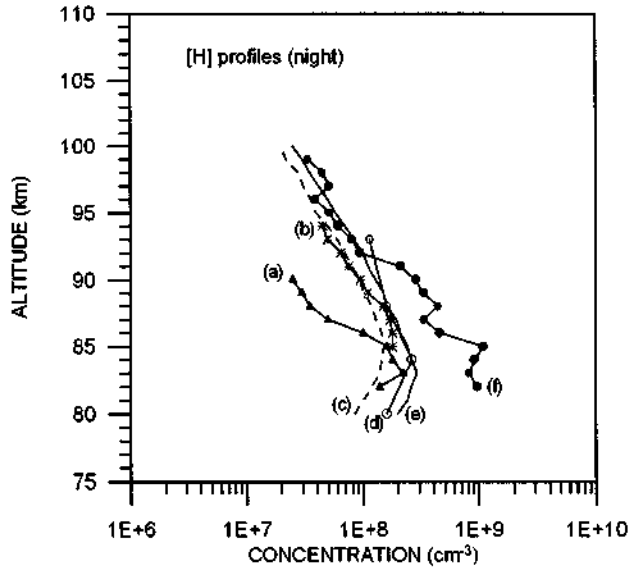

Figure 7 Observed and model [H] profiles (nighttime): (a) *Ulwick et al.* [1987] (observation); (b) *Adler-Golden et al.* [1992] (observation); (c) *Sharp and Kita* [1987] (observation); (d) *Thomas* [1990a] (observation); (e) *Allen et al.* [1984] (model); (f) present results.

determined [O_3] from its 9.6 μm emission and [O] by the resonance lamp technique. The hydrogen concentration was then obtained from the O_3 - H equilibrium condition. On the basis of SME data, *Thomas* [1990a] inferred [O_3] from the $O_2(^1\Delta_g)$ 1.27 μm emission and [H] using the same technique. The [H] values plotted in Figure 7 are for the month of May at the equator and were taken from Table 2 of the Thomas paper. Recently, *Adler-Golden et al.* [1992] inferred [H] from the ozone infrared emission. The only model profile shown is that due to *Allen et al.* [1984]. Although these [H] profiles were obtained at different seasons and latitudes, using different techniques, there is fairly good agreement between them. Number density varies from 2 x 10^8 cm^{-3} at around 82 km to 5 x 10^7 cm^{-3} at 95 km. The present results show good agreement with these profiles above 92 km, but below 90 km, our values are considerably larger than the others, with a discrepancy of about a factor of 4 at 85 km.

The large hydrogen concentration below 90 km merits some discussion. From the SME satellite data [*Thomas*, 1990a], taken in the equatorial region, it can be seen that [H] and [O_3] both show a strong semiannual variation, with maximum [H] and minimum [O_3] in June/July and December/January. The present rocket data were taken at the end of May, the season when [H] would be expected to be moving toward maximum and [O_3] toward minimum. Therefore the present data suggest that when [H] increases during the solstice, the major change occurs below 90 km. This could be the result of greater vertical transport of water vapor, and subsequent photodissociative production of atomic hydrogen, in the equatorial region. The strong semiannual variations observed in the NaD and OI 557.7 nm airglow emission intensities [*Kirchhoff and Takahashi*, 1985; *Takahashi et al.*, 1994], which have been attributed to seasonal variations in the dynamics of the upper atmosphere, are also consistent with this suggestion.

In conclusion, height variations of the nighttime ozone and hydrogen concentrations, derived from simultaneous measurements of the Na density profile and the NaD and OH(8,3) band emissions in the equatorial region, are in general agreement with measurements made at other latitudes. The absolute value of the hydrogen concentration is, however, much larger in the height region below 90 km. Uncertainty in the branching ratio α for the reaction NaO + O → Na(^{2}P) + O_2, believed to be responsible to the production of excited sodium, is a limiting factor in the precision of the determination of the absolute values for [O_3] and [H]. A more reliable laboratory determination of the value of α applicable to the NaO + O reaction in the atmosphere is necessary. A direct simultaneous measurement of the vertical profiles of ozone, Na, and the NaD airglow intensity would also help to resolve this question.

Acknowledgments. The present rocket experiment was carried out in cooperation with the Instituto de Aeronáutica e Espaço (IAE) and the Alcântara Launch Center. The authors are grateful to the many people who made this work possible. This work was partially supported by the Conselho Nacional de Desenvolvimento Científico e Tecnológico (CNPq), under contracts 300675/90-9 and 300609/94-9.

References

Adler-Golden, S. M., J. Gruninger, and D. R. Smith, Derivation of atmospheric oxygen and hydrogen profiles from ozone ν_3 band emission, *J. Geophys. Res.*, *97*, 19,509-19,518, 1992.

Allen, M., J. I. Lunine, and Y. L. Yung, The vertical distribution of ozone in the mesosphere and lower thermosphere, *J. Geophys. Res.*, *89*, 4841-4872, 1984.

Bates, D. R., and P. C. Ojha, Excitation of the NaD doublet of the nightglow, *Nature*, *286*, 790-791, 1980.

Chalamala, B. R., and R. A. Copeland, Collision dynamics of OH(X, v=9), *J. Chem. Phys.*, *99*, 5807 - 5811, 1993.

Chapman, S., Notes on atmospheric sodium, *Astrophys. J.*, *90*, 309-316, 1939.

Clemesha, B. R., and H. Takahashi, Rocket-borne measurements of horizontal structure in the OH(8,3) and NaD airglow emissions, *Adv. Space Res.*, 17(11), 81-84, 1995.

Clemesha, B. R., H. Takahashi, and Y. Sahai, Vehicle glow observed during a rocket sounding experiment, *Planet. Space Sci.*, *35*, 1367-1372, 1987.

Clemesha, B. R., D. M. Simonich, H. Takahashi, and S. M. L. Melo, A simultaneous measurement of the vertical profiles of sodium nightglow and atomic sodium density in the upper atmosphere, *Geophys. Res. Lett.*, *20*, 1347-1350, 1993.

Clemesha, B. R., D. M. Simonich, H. Takahashi, S. M. L. Melo, and J. M. C. Plane, Experimental evidence for photochemical control of the atmospheric sodium layer, *J. Geophys. Res.*, 100, 18,909-18,916, 1995.

DeMore, W. B., et al., Chemical kinetics and photochemical data for use in stratospheric modeling, in Evaluation 8., *JPL Publ. 87-41*, Jet Propul. Lab., Passadena, California,1987.

Dickinson, P. H. G., W. C. Bain, L. Thomas, E. R. Williams, D. B. Jenkins, and N. D. Twiddy, The determination of the atomic oxygen concentration and associated parameters in the lower ionosphere, *Proc. R. Soc. Lond.*, *369*, 379-408, 1980.

Finlayson-Pitts, B. J., and T. E. Kleindienst, The reaction of hydrogen atoms with ozone as a source of vibrationally excited OH(X) for kinetic studies, *J. Chem. Phys.*, *74*, 5643 - 5658, 1981.

Garcia, R. R., and S. Solomon, The effect of breaking gravity waves on the dynamics and chemical composition of the mesosphere and lower thermosphere, *J. Geophys. Res.*, *90*, 3850-3868, 1985.

Greer, R. G., et al., ETON 1: A data base pertinent to the study of energy transfer in the oxygen nightglow, *Planet. Space Sci.*, *34*, 771-788, 1986.

Grossmann, K. U., et al., Middle atmosphere abundances of water vapor and ozone during MAP/WINE, *J. Atmos. Terr. Phys.*, *49*, 827-841, 1987.

Herschbach, D. R., C. E. Kolb, D. R. Worsnop, and X. Shi, Excitation mechanism of the mesospheric sodium nightglow, *Nature*, *356*, 414-416, 1992.

Johnston, J. E., and A. L. Broadfoot, Midlatitude observations of the

night airglow: Implications to quenching near the mesopause, *J. Geophys. Res., 98*, 21,593-21,603, 1993.

Kirchhoff, V. W., J. H. and H. Takahashi, First sodium nightglow results for Natal, *Planet. Space Sci., 33*, 757-760, 1985.

Kirchhoff, V. W. J. H., B. R. Clemesha, and D. M. Simonich, Seasonal variation of ozone in the mesosphere, *J. Geophys. Res., 86*, 1463-1466, 1981.

Kolb, C. E., and J. B. Elgin, Gas phase chemical kinetics of sodium in the upper atmosphere, *Nature, 263*, 488-490, 1976.

Lin, C. L., and M. T. Leu, Temperature and third body dependence of the rate constant for the reaction $O + O_2 + M \rightarrow O_3 + M$, Int. *J. Chem. Kinet., 14*, 417, 1982.

McDade, I. C., and E. J. Llewellyn, Mesospheric oxygen atom densities inferred from nighttime OH Meinel band emission rates, *Planet. Space Sci., 36*, 897-905, 1988.

McDade, I. C., D. P. Murtagh, R. G. H. Greer, P. H. G. Dickinson, G. Witt, J. Stegman, E. J. Llewellyn, L. Thomas, and D. B. Jenkins, ETON 2: Quenching parameters for the proposed precursors of $O_2(b^1\Sigma_g^+)$ and $O(^1S)$ 557.7 nm in the terrestrial nightglow, *Planet. Space Sci., 34*, 789, 1986a.

McDade, I. C., E. J. Llewellyn, R. G. H. Greer, and D. P. Murtagh, ETON 3: Altitude profiles of the nightglow continuum at green and near infrared wavelengths, *Planet. Space Sci., 34*, 801-810, 1986b.

McDade, I. C., E. J. Llewellyn, D. P. Murtagh, and R. G. H. Greer, ETON 5: Simultaneous rocket measurements of the OH Meinel (8,3) band and $\Delta v = 2$ sequence in the nightglow, *Planet. Space Sci., 35*, 1137, 1987.

Melo, S. M. L., H. Takahashi, B. R. Clemesha, P. P. Batista, and D. M. Simonich, Atomic oxygen concentrations from rocket airglow observations in the equatorial region, *J. Atmos. Terr. Phys.*, in press, 1995.

Murphy, R. E., Infrared emission of OH in the fundamental and first overtone bands, *J. Chem. Phys., 54*, 4852-4859, 1971.

Murtagh, D. P., R. G. H. Greer, I. C. McDade, E. J. Llewellyn and M. Bantle, Representative Volume Emission Profiles from Rocket Photometer Data, *Ann. Geophys., 2*, 467-474, 1984.

Murtagh, D. P., G. Witt, J. Stegman, I. C. McDade, E. J. Llewellyn, F. Harris, and R. G. H. Greer, An assessment of proposed $O(^1S)$ and $O_2(b^1\Sigma_g^+)$ nightglow excitation parameters, *Planet. Space Sci., 38*, 43-53, 1990.

Ohoyama, H., T. Kasai, Y. Yoshimura, H. Kimura, and K. Kuwata, Initial distribution of vibration of the OH radicals produced in the $H + O_3 = OH(X^2\Pi) + O_2$ reaction chemiluminescence by a crossed beam technique, *Chem.Phys. Lett., 118*, 263-267, 1985.

Plane, J. M. C., and D. Husain, Determination of the absolute rate constant for the reaction $NaO + O \rightarrow Na + O_2$ by time-resolved atomic chemiluminescence at lambda = 589 nm [$Na(3\ ^2P_1) \rightarrow Na(3\ ^2S_{1/2}) + h\nu$], *J. Chem. Soc., 82*, 2047-2052, 1986.

Plane, J. M. C., C. F. Nien, M. R. Allen, and M. Helmer, A kinetic investigation of the reactions $Na + O_3$ and $NaO + O_3$ over the temperature range 207-377 K, *J. Phys. Chem., 97*, 4459-4467, 1993.

Sharp, W. E., and D. Kita, In situ measurement of atomic hydrogen in the upper mesosphere, *J. Geophys. Res., 92*, 4319-4324, 1987.

Takahashi, H., and P. P. Batista, Simultaneous measurements of OH(9,4), (8,3), (7,2), (6,2) and (5,1) bands in the airglow, *J. Geophys. Res.*, 86, 5632, 1981.

Takahashi, H., B. R. Clemesha, Y. Sahai, P. Batista, and D. M. Simonich, Seasonal variations of mesospheric hydrogen and ozone concentrations derived from ground-based airglow and lidar observations, *J. Geophys. Res., 97*, 5987, 1992.

Takahashi, H., B. R. Clemesha, and P. P. Batista, Predominant semi-annual oscillation of the upper mesospheric airglow intensities and temperatures in the equatorial region, *J. Atmos. Terr. Phys., 57*, 407-414, 1994.

Thomas, R. J., Atomic hydrogen and atomic oxygen density in the mesopause region: Global and seasonal variations deduced from Solar Mesosphere Explorer near-infrared emissions, *J. Geophys. Res., 95*, 16,457-16,476, 1990a.

Thomas, R. J., Seasonal ozone variations in the upper mesosphere, *J. Geophys. Res., 95*, 7395-7401, 1990b.

Thomas, R. J., and R. . Young, Measurements of atomic oxygen and relaated airglow in the lower thermosphere, *J. Geophys. Res., 86*, 7389-7393, 1981.

Turnbull, D. N., and R. P. Lowe, New hydroxyl transition probabilities and their importance in airglow studies, *Planet. Space Sci., 37*, 723-738, 1989.

Ulwick, J. C., K. D. Baker, D. J. Baker, A. J. Steed, P. J. W.R., K. Grossmann, and H. G. Bruckelmann, Mesospheric minor species determinations from rocket and ground-based i.r. measurements, *J. Atmos. Terr. Phys., 49*, 855-862, 1987.

Vaughan, G., Diurnal variation of mesospheric ozone, *Nature, 296*, 133-135, 1982.

Worsnop, D. R., M. S. Zahniser, and C. E. Kolb, Low-temperature absolute rate constants for the reaction of atomic sodium with ozone and nitrous oxide, *J. Phys. Chem., 95*, 3960-3964, 1991.

B. R. Clemesha, S. M. L. Melo, D. M. Simonich, and H. Takahashi, INPE, C.P. 515, São.José. dos Campos, São Paulo 12201-970, Brazil. (e-mail: inpedaa@eu.ansp.br)

J. Stegman and G. Witt, Meteorology Department, Stockholm University, S 10691 Stockholm, Sweden

(Received June 28, 1994; revised July 13, 1995;
accepted September 19, 1995.)